Critical dynamics of the body-centered-cubic classical Heisenberg antiferromagnet

Alex Bunker, Kun Chen,* and D. P. Landau
Center for Simulational Physics, University of Georgia, Athens, Georgia 30602
(Received 15 April 1996)

We have used spin dynamics techniques to perform large-scale simulations of the dynamic behavior of the $L\times L\times L$ body-centered-cubic classical Heisenberg antiferromagnet with $L\leqslant 48$ at a range of temperatures above and below as well as at the critical point T_c. The temporal evolutions of the spin configurations were determined numerically from coupled equations of motion for individual spins by a fourth-order predictor-corrector method, with initial spin configurations generated by Monte Carlo simulations. The neutron scattering function $S(q,\omega)$ was calculated from the space- and time-displaced spin-spin correlation function. We used a previously developed dynamic finite-size scaling theory to extract the dynamic critical exponent z from $S(q,\omega)$ at T_c. Our results are in agreement with the theoretical prediction of $z=1.5$ and with experimental results; however, we find that the asymptotic regime was only entered at $L\approx 30$. In the analysis of the form of the transverse and longitudinal components of $S(q,\omega)$ we found that a central diffusion peak appears below T_c predominantly in the longitudinal component and remains present through and above T_c. The transverse component of the spin-wave peak is Lorentzian below T_c but for $T\geqslant T_c$ is described best by a more complex functional form. Below T_c we see evidence of multiple spin-wave peaks in the longitudinal component. [S0163-1829(96)02138-8]

I. INTRODUCTION

The isotropic Heisenberg antiferromagnet has the same static critical behavior as the ferromagnet which has been studied using a variety of approaches including a recent high-resolution Monte Carlo study.[1] This work determined the critical temperature and the static critical exponents for the simple cubic and body-centered-cubic systems to a precision equivalent to or better than that found with any other method and substantiated the hypothesis of universality for static properties once again. The theory of the dynamic behavior of the Heisenberg model is, however, not so clearly understood. The dynamics of the Heisenberg antiferromagnet is very different from that of the ferromagnet since the order parameter (the staggered magnetization) is no longer a conserved quantity. One only needs to look to linear spin-wave theory to see that the low-temperature dispersion curves are markedly different for the two models. Dynamic critical behavior is describable in terms of a dynamic critical exponent z which is dependent on conservation laws, lattice dimension, and the static critical exponents. In their work on the theory of dynamic critical phenomena,[2] Hohenberg and Halperin proposed a number of different dynamic universality classes based upon the conservation laws. The classical Heisenberg ferromagnet and antiferromagnet are of class J and G, respectively; both of these classes have true dynamics with spin variables of continuous degrees of freedom and real time dynamic behaviors governed by coupled equations of motion. The difference between the classes is that the order parameter is only conserved in class J. Using dynamic scaling they found that $z=3-\beta/\nu$ for class J, and various theoretical methods[2–5] were used to determine that $z=d/2$ for class G where β and ν are the static critical exponents and d is the dimension of the system.

The material which is best described by the isotropic antiferromagnetic Heisenberg Hamiltonian is $RbMnF_3$. Early experimental studies[6–8] have shown that it has a simple cubic lattice structure with a nearest-neighbor exchange constant of $J=0.58\pm 0.06$ meV and a second-neighbor constant of less than 0.04 meV [both defined using our convention for J as defined in Eq. (1)]. The critical point was found to be 83 K, which makes the study of the critical region amenable to neutron scattering experiments. The magnetic anisotropy was found to be only 4.5 G, and no deviation from cubic symmetry was seen to occur at T_c. Neutron scattering experiments have been carried out on $RbMnF_3$ by Tucciarone *et al.*[9] who found that in the critical region the neutron scattering function was found to have a central peak (peak at frequency $\omega=0$) as well as a spin-wave peak. This central peak is thought to be due to spin diffusion resulting from nonlinearities in the dynamical equations.[10] Two-crystal neutron scattering revealed static critical exponents in agreement with theory and a three-crystal neutron scattering measurement found a value of the dynamic critical exponent slightly lower than but still within the error bars of the theoretical prediction of $z=1.5$. Another more recent study by Cox *et al.*[11] indicates the presence of a small central peak below T_c.

In this paper we present results of large-scale computer simulations of the dynamic behavior for the Heisenberg antiferromagnet. We focus mainly on the critical region but also have found results for temperatures above and below the critical point. In Sec. II we define the model and discuss dynamic scaling theory, and in Sec. III we present and discuss our simulation results.

II. MODEL AND METHODS

A. Model

The classical Heisenberg antiferromagnet is defined by the Hamiltonian

$$\mathcal{H}=J\sum_{\langle \mathbf{r}\mathbf{r}'\rangle}\mathbf{S}_{\mathbf{r}}\cdot\mathbf{S}_{\mathbf{r}'}, \tag{1}$$

where $\mathbf{S}_{\mathbf{r}}=(S_r^x,S_r^y,S_r^z)$ is a three-dimensional classical spin of unit length at site $\mathbf{r}$ and $J>0$ is the antiferromagnetic coupling constant between nearest-neighbor spins. We consider $L\times L\times L$ body-centered-cubic systems with periodic boundary conditions. The dynamics of the spins will be governed by the coupled equations of motion,

$$\frac{d}{dt}\mathbf{S}_{\mathbf{r}}=-\mathbf{S}_{\mathbf{r}}\times J\sum_{\langle \mathbf{r}\mathbf{r}'\rangle}\mathbf{S}_{\mathbf{r}'}, \tag{2}$$

and the time dependence of each spin can be determined from the integration of these equations.

B. Dynamic scaling

The neutron scattering function $S(\mathbf{q},\omega)$ for momentum transfer $\mathbf{q}$ and frequency transfer ω is an experimental observable and is fundamental to the study of spin dynamics. It is given by

$$S^k(\mathbf{q},\omega)=\sum_{\mathbf{r},\mathbf{r}'}\exp[i\mathbf{q}\cdot(\mathbf{r}-\mathbf{r}')]\times\int_{-\infty}^{+\infty}\exp(i\omega t)C^k(\mathbf{r}-\mathbf{r}',t)\frac{dt}{\sqrt{2\pi}}. \tag{3}$$

$C^k(\mathbf{r}-\mathbf{r}',t)$ is the space-displaced, time-displaced spin-spin correlation function defined, with $k=x$, y, or z, as

$$C^k(\mathbf{r}-\mathbf{r}',t)=\langle S_{\mathbf{r}}^k(t)S_{\mathbf{r}'}^k(0)\rangle-\langle S_{\mathbf{r}}^k(t)\rangle\langle S_{\mathbf{r}'}^k(0)\rangle. \tag{4}$$

The displacement $\mathbf{r}$ is in units of the lattice unit cell length a. For the ferromagnetic case $S_{\mathbf{r}}^k(t)$ is the value of the k component of the spin at position $\mathbf{r}$ and time t. For the antiferromagnetic case the lattice can be divided into sublattices A and B, where in the ordered state the spins in sublattice B point in the opposite direction to the spins in sublattice A. For the spins on sublattice B, $S_{\mathbf{r}}^k(t)$ will be the negative of the spin value at that site.

The neutron scattering function can be written in the form[12]

$$S_\xi^k(\mathbf{q},\omega)=\frac{2\pi}{\omega_m(\mathbf{q},\xi)}\chi_\xi^k(\mathbf{q})f\left(\frac{\omega}{\omega_m(\mathbf{q},\xi)},\mathbf{q},\xi\right), \tag{5}$$

where ξ is the correlation length, $\chi_\xi^k(\mathbf{q})$ is momentum-dependent susceptibility given by

$$\int_{-\infty}^{\infty}S_\xi^k(\mathbf{q},\omega)\frac{d\omega}{2\pi}=\chi_\xi^k(\mathbf{q}), \tag{6}$$

and f is the normalized form function. The characteristic frequency $\omega_m(\mathbf{q},\xi)$ is a median frequency determined by the constraint

$$\int_{-\omega_m(\mathbf{q},\xi)}^{\omega_m(\mathbf{q},\xi)}S_\xi^k(\mathbf{q},\omega)\frac{d\omega}{2\pi}=\frac{1}{2}\chi_\xi^k(\mathbf{q}). \tag{7}$$

The characteristic frequency can be seen as a generalized halfwidth of $S(\mathbf{q},\omega)$. In the dynamic scaling theory it is assumed that $\omega_m(\mathbf{q},\xi)$ is a homogeneous function of q and ξ, i.e.,

$$\omega_m(\mathbf{q},\xi)=q^z\Omega(q\xi), \tag{8}$$

where z is the dynamic critical exponent, and that f, the form function, depends only on the product of $q\xi$ but not on $\mathbf{q}$ and ξ separately. Therefore $S_\xi^k(\mathbf{q},\omega)$ as given in Eq. (5) is simplified,

$$S_\xi^k(\mathbf{q},\omega)=\frac{2\pi}{\omega_m(q\xi)}\chi_\xi^k(\mathbf{q})f\left(\frac{\omega}{\omega_m(q\xi)},q\xi\right). \tag{9}$$

C. Form function

The form functions for both magnetic, f_M, and staggered magnetic, f_N, correlations as a function of $q\xi$ have been predicted for the isotropic antiferromagnet through the use of renormalization group methods.[4,13] For high enough temperature, the relaxation regime, where $q\xi\ll 1$, f_N should be a simple Lorentzian centered around the origin $\omega=0$. As the temperature decreases and we approach the critical regime, $q\xi\gg 1$ and two spin-wave peaks appear displaced symmetrically about the origin. The positions of the peak moves outward as $q\xi$ increases until a limiting value is reached as the critical region is approached. f_M remains Lorentzian for $T\geqslant T_c$. Below T_c the renormalization group theory becomes more approximate due to complications arising from the presence of an ordered phase. It can only predict that a spin-wave peak exists and that it will become broader as temperature increases. We know from linear spin-wave theory that, in the $(q,0,0)$ direction, for Heisenberg spins as $T\to 0$ the central peak vanishes and the spin-wave peak becomes sharper, approaching a δ function at $\omega=8\sin(q/2)$ for the bcc lattice and $\omega=4\sin(q/2)[2+\cos^2(q/2)]^{1/2}$ for the simple-cubic lattice. Renormalization group theory does not distinguish between the two lattice structures in making predictions.

D. Simulational background

Using a combination of Monte Carlo and spin dynamics methods,[14,15] we simulated the behavior of the body-centered-cubic classical Heisenberg antiferromagnet with $8\leqslant L\leqslant 48$ at the critical point $T_c=2.054\,241J$, where we have chosen units such that the Boltzmann constant $k=1$. We also examined the behavior outside the critical region, at slightly above the critical point, $T=2.1J$, and at a set of temperatures below T_c, $T=1.0J$, $1.3J$, $1.5J$, and $1.9J$, with $L=32$. All simulations were carried out on the Cray C90 at the Pittsburgh Supercomputing Center.

We used the same hybrid Monte Carlo method as Chen and Landau[14] in the study of the critical dynamics of the Heisenberg ferromagnet to generate equilibrium configurations. A single hybrid Monte Carlo step consisted of two Metropolis steps and eight overrelaxation steps. Typically 1000 hybrid MC steps were used to generate each equilibrium configuration. Our spin dynamics method differed only in that we carried out the integration to a larger time $t_{\max}=200J^{-1}$ instead of, as in the previous study,

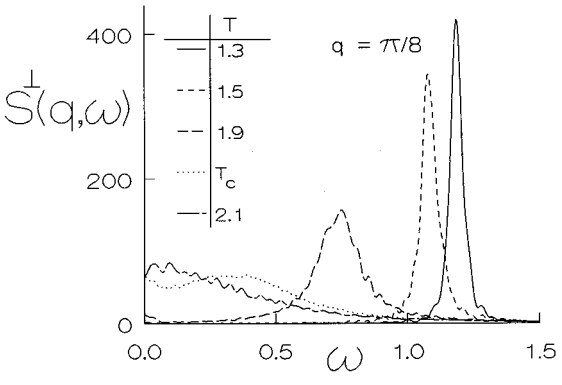

FIG. 1. Graph of $S^{\perp}(\mathbf{q},\omega)$ for $q=\pi/8$ at $T=1.3J$, $T=1.5J$, $T=1.9J$, $T=T_c$ (2.054 241J), and $T=2.1J$ showing the broadening and decrease in frequency of the spin-wave peak as temperature increases.

$t_{\max}=120J^{-1}$. We also used the technique of calculating partial spin sums ''on the fly'' which limits us to data in the $(q,0,0)$ direction with q determined by the periodic boundary conditions,

$$q=\frac{2\pi n}{L}, \quad n=\pm 1,\pm 2,\ldots,\pm(L-1),L. \tag{10}$$

We used the fast Fourier transform (FFT) algorithm to increase the efficiency of the program. The time-displaced, space-displaced spin-spin correlation function was calculated from an average over 200 different time starting points evenly spaced by $0.1J^{-1}$ for a time period $0\leqslant t\leqslant t_{\text{cutoff}}$ with $t_{\text{cutoff}}=180J^{-1}$. The resolution of our results in ω is limited by the finite time cutoff according to the relation

$$\delta\omega=\frac{1.2\pi}{t_{\text{cutoff}}}. \tag{11}$$

(The factor of 1.2π results from the difference between the half-width and σ.) In our case $\delta\omega\approx 0.021$. Since all three Cartesian spatial directions are equivalent by symmetry, the same operation carried out for the $(q,0,0)$ direction was also carried out for the other two reciprocal lattice directions $(0,q,0)$ and $(0,0,q)$ and the results were averaged.

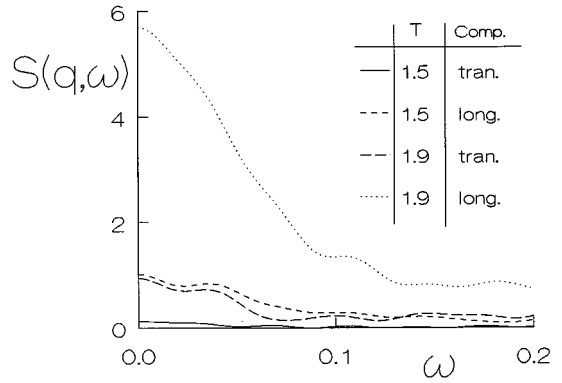

FIG. 2. Graph of the low ω part of $S^{\perp}(\mathbf{q},\omega)$ and $S^{\parallel}(\mathbf{q},\omega)$ for $q=3\pi/16$ at $T=1.5J$ and $T=1.9J$ showing the presence of a central peak in the ordered phase which increases with increasing temperature. We see that the central peak has a more intense longitudinal than transverse component. The oscillations seen are caused by the finite time cutoff.

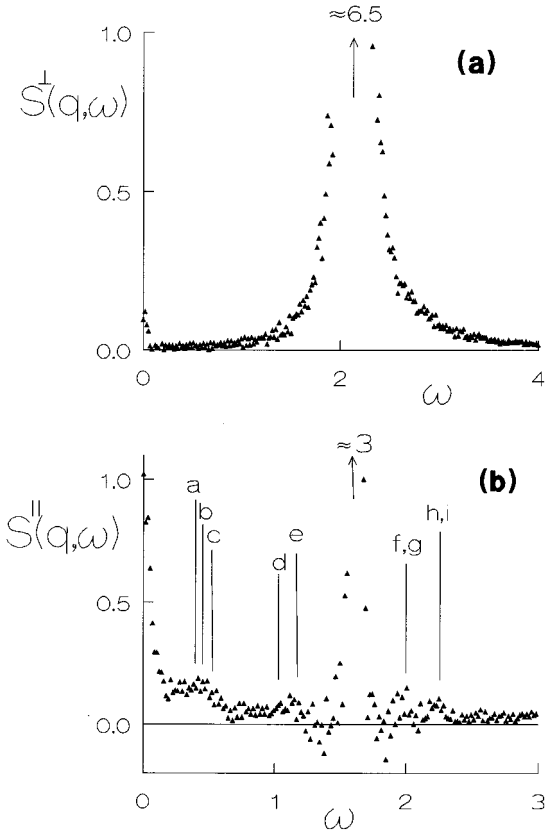

FIG. 3. Graphs of $S^{\perp}(\mathbf{q},\omega)$ and $S^{\parallel}(\mathbf{q},\omega)$ for $T=1.5J$ and $q=3\pi/16$. We see possible multiple spin-wave peaks which are only present in the longitudinal component. We found predicted two-spin wave peaks to match our results only for the case of spin waves on the simple cubic subset of the fcc reciprocal lattice. The approximated two-spin waves labeled are (a) $(2,-1,-1)$, (b) $(2,-1,0)$, (c) $(2,0,0)$, (d) $(3,-1,-1)$, (e) $(3,-1,0)$, (f) $(3,-1,-1)$, (g) $(2,-1,0)$, (h) $(3,-1,0)$, and (i) $(2,-1,-1)$.

While the original study of Chen and Landau[14] used 100 equilibrium spin configurations for lattice sizes up to $L=40$, we used 1000 equilibrium spin configurations for lattice sizes $L=8-32$ and 400 equilibrium spin configurations for lattice sizes $L=40$ and 48.

We also averaged results for spin components $k=x$ and y, since the staggered magnetization is a conserved vector along the z direction in spin space so that the neutron scattering function $S^{k}_{\xi}(\mathbf{q},\omega)$ can be regrouped in terms of symmetry as a longitudinal component

$$S^{\parallel}(\mathbf{q},\omega)=S^{z}(\mathbf{q},\omega) \tag{12}$$

and a transverse component

$$S^{\perp}(\mathbf{q},\omega)=\frac{1}{2}[S^{x}(\mathbf{q},\omega)+S^{y}(\mathbf{q},\omega)], \tag{13}$$

where the spins are reoriented so that the direction of the order parameter, staggered magnetization, remains parallel to the z axis.

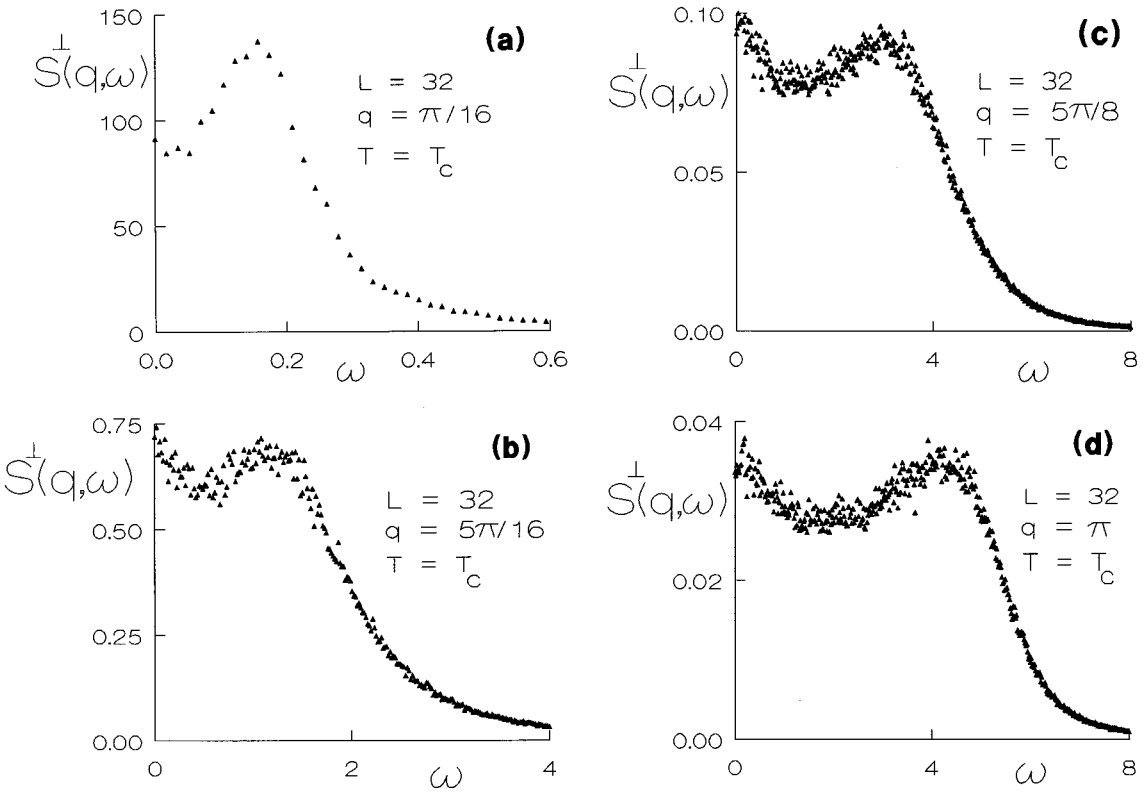

FIG. 4. Graphs of $S^{\perp}(\mathbf{q},\omega)$ at $T=T_c$ for lattice size $L=32$ over the range of q values, $q=\pi/16$, $5\pi/16$, $5\pi/8$, and π.

E. Dynamic finite-size scaling

We used a previously developed dynamic finite-size scaling theory[14,16] in order to extract an estimate for the dynamic critical exponent z. Since the finite time cutoff was only $100J^{-1}$ for the ferromagnet, oscillations were introduced into the result of the Fourier transform which had to be smoothed out by convoluting the spin correlation function with a resolution function in frequency. We found that by taking the finite time cutoff out to $180J^{-1}$ these oscillations became negligible and we could perform the finite-size scaling analysis without the use of a resolution function. As a result the dynamic finite-size scaling relations[14,16] simplify to

$$\frac{S_L^k(\mathbf{q},\omega)}{L^z\chi_L^k(\mathbf{q})}=G(\omega L^z,qL) \tag{14}$$

and

$$\omega_m(\mathbf{q},L)\equiv\omega_m(qL)=L^{-z}\overline{\Omega}(qL). \tag{15}$$

$S_L^k(\mathbf{q},\omega)$ is the calculated neutron scattering function at lattice size L, $\chi_L^k(\mathbf{q})$ is given by

$$\int_{-\infty}^{\infty}S_L^k(\mathbf{q},\omega)\frac{d\omega}{2\pi}=\chi_L^k(\mathbf{q}), \tag{16}$$

and $\omega_m(qL)$, the characteristic frequency, is given by

$$\int_{-\omega_m(qL)}^{+\omega_m(qL)}S_L^k(\mathbf{q},\omega)\frac{d\omega}{2\pi}=\frac{1}{2}\chi_L^k(\mathbf{q}). \tag{17}$$

We can thus test dynamic scaling and estimate the dynamic critical exponent z. Simpson's rule was used to carry out the integration in order to determine the characteristic frequency.

We see that a value for z can be obtained from the slope of a graph of $\log\omega_m$ vs $\log L$ if the value of qL is fixed; however, this will only give us the correct answer if all the lattice sizes included in the calculation are large enough to be in the asymptotic-size regime. The approximate lattice size of the onset of the asymptotic regime can be seen by comparing ωL^z values for the different lattice sizes for a trial value of z. If z is chosen correctly, then for fixed qL, due to the first scaling relation [Eq. (14)], graphs of $S_L^k(\mathbf{q},\omega)/L^z\chi_L^k(\mathbf{q})$ vs ωL^z should all fall onto the same curve for lattice sizes in the asymptotic regime. This can be used as a test for our solution of z.

III. RESULTS

A. Data for $S(q,\omega)$

Our results at the temperatures below T_c show, as expected, the spin-wave peak becoming narrower and increasing in frequency, approaching linear spin-wave theory as temperature decreases. Figure 1 shows a comparison of the $q=\pi/8$ transverse spin-wave peaks for five of the temperatures studied. Our peak widths even for $T=1.0J$ are wide enough that the contribution due to the finite resolution is negligible. The high-frequency oscillations present in the data are only due to the finite time cutoff at low T and q. At higher T and q values these are mostly due to noise in the data. The longitudinal and transverse spin waves are at the same frequency, and thus we see no evidence of the phenom-

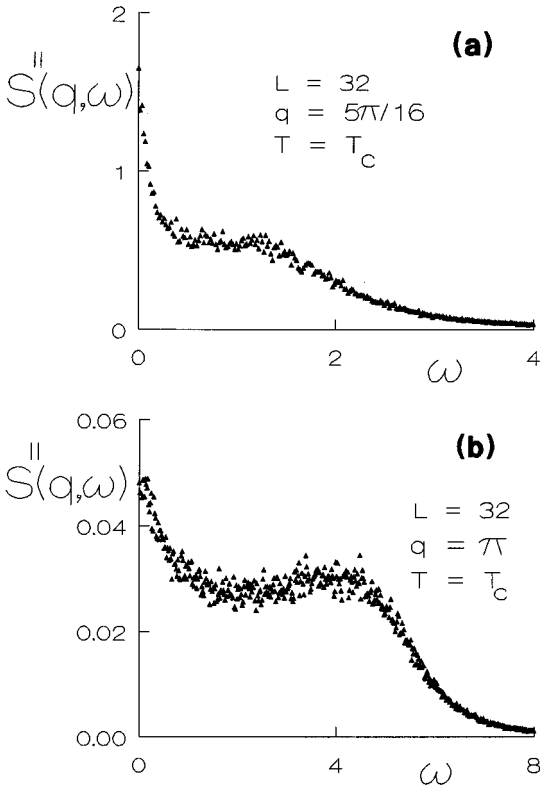

FIG. 5. Graphs of $S^{\parallel}(\mathbf{q},\omega)$ at $T=T_c$ for lattice size $L=32$ at the q values $q=5\pi/16$ and $q=\pi$. In comparison to the transverse component the central diffusion peak is much stronger and the spin-wave peak is less intense.

enon of ''second sound''; however, the spin-wave peak is much less intense in the longitudinal component than in the transverse component. This is to be expected since according to linear spin-wave theory longitudinal exitations vanish as $T\rightarrow 0$. As the zone boundary is approached the form of the transverse spin-wave peak becomes increasingly asymmetric, deviating from a qualitatively lorentzian form.

We see the existence of a central peak that is increasing in strength with increasing temperature and is much more intense in the longitudinal than in the transverse component as shown in Fig. 2. The central peak decreases less with increasing q than the spin-wave peak and for the longitudinal component becomes the dominant exitation as the zone boundary is approached. Our results showing the existence of a central peak below T_c are in agreement with the experimental results of Cox *et al.*[11]

We also see possible evidence of multiple spin-wave peaks which are most clearly seen at $T=1.5J$ as shown in Fig. 3. These are only present in the longitudinal component and broaden as $T\rightarrow T_c$, becoming indistinguishable as separate exitations. If we make the assumptions that the dominant multiple spin-wave exitations are two-spin waves, then we can estimate the frequencies of possible multiple spin-wave peaks. Restricting ourselves to sites on the reciprocal lattice which are in the vicinity of the single spin-wave vector we are left with a set of predicted multiple spin-wave frequencies that we can match to our results as indicated in Fig. 3. We only see spin-wave peaks corresponding to two-spin waves which are combinations of spin waves on the simple

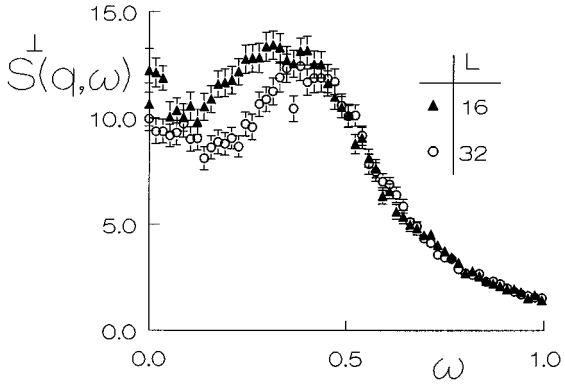

FIG. 6. Graph of $S^{\perp}(\mathbf{q},\omega)$ for $q=\pi/8$ and $T=T_c$ showing the finite-size effects at lattice size $L=16$ in comparison to the result at lattice size $L=32$ which is in the asymptotic regime.

cubic subset of the reciprocal fcc lattice that the beginning and end point of the two-spin wave belong and do not see that same agreement for other two-spin wave combinations.

Figures 4 and 5 show transverse, $S^{\perp}(\mathbf{q},\omega)$, and longitudinal, $S^{\parallel}(\mathbf{q},\omega)$, components of $S(\mathbf{q},\omega)$ at $T=T_c$ at a set of q values. The longitudinal component is similar in form to that of the Heisenberg ferromagnet.[14] As is the case for $T<T_c$ there is a much stronger central diffusion peak in the longitudinal component than in the transverse component. The spin-wave peak of the longitudinal component is also weaker than in the transverse component. Theoretically at T_c one should not be able to separate the longitudinal and transverse components but due to finite-size effects a residual magnetization is present which causes the difference between these two components.

Our results for $S^{\perp}(\mathbf{q},\omega)$ are in qualitative agreement with the experimental results[9] in that we see the expected central peak as well as a spin-wave peak; however, they are in stark disagreement with theoretical (coupled-mode theory) results[5] which predict a minimum at $\omega=0$. When q is increased we see a uniform decrease in intensity and a combined frequency increase and broadening of the spin-wave peak. While over most q values the relative intensity of the central and spin-wave peaks remains a constant, at very small q the relative intensity of the central peak decreases. Note that as we move from small q to the zone boundary the intensity changes by four orders of magnitude, yet we still have rather good resolution in the data. When we compare $S^{\perp}(\mathbf{q},\omega)$ for the different lattice sizes we see that finite-size effects extend to a higher lattice size for the central peak than for the spin-wave component. There is no noticeable finite-size effect for lattice sizes $L=32$ and above for the case of small q (where the contribution due to the central peak is negligible). This indicates that this is the lower bound of the asymptotic regime. In Fig. 6 we see the finite-size effects present for lattice size $L=16$. The spin-wave peak is shifted to slightly higher frequency and the central peak is reduced and broadened.

When we increase the temperature to $T=2.1J$, slightly above T_c, $S(\mathbf{q},\omega)$ is completely isotropic and shows a broader and stronger central peak and a broader spin-wave peak centered at a lower frequency than the result at T_c. This lowering of the frequency of the spin-wave peak is pre-

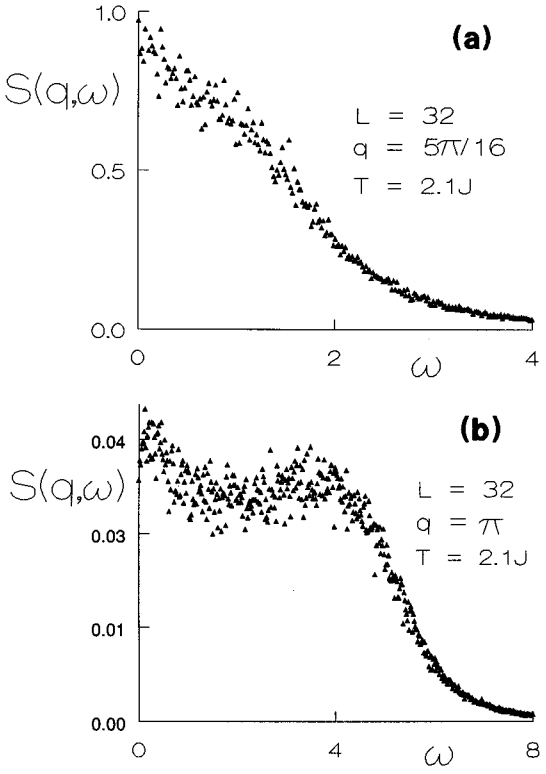

FIG. 7. Graph of $S(\mathbf{q},\omega)$ at $T=2.1J$ for lattice size $L=32$ at the q values $q=5\pi/16$ and $q=\pi$. We see that the spin-wave peak is obscured by the central peak at the low q value.

dicted by renormalization group theory[4] pertaining to the form function in the vicinity of the critical region. In Fig. 7 we see that at low q the spin-wave peak is not discernible due to the increased width and strength of the central peak. At higher q a spin-wave peak is discernible but is very broad and is still masked by the central peak.

We were able to plot approximate dispersion curves at T_c. Figure 8 shows a comparison of the dispersion curve to the low-temperature ($T=0.1J$) dispersion curve which approximately matches linear spin-wave theory. The dispersion

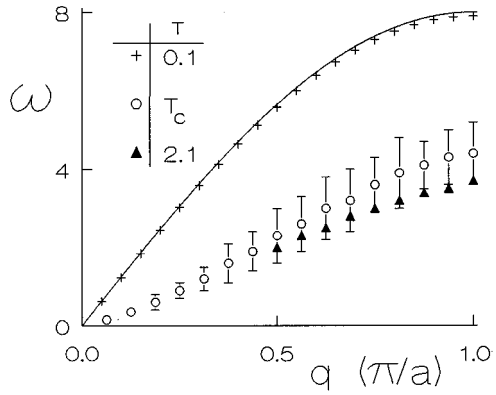

FIG. 8. Graph of dispersion curves at $T=0.1J$ where behavior closely matches linear spin-wave theory ($T=0$, the solid line) compared to our results at T_c and $T=2.1J$. The error bars for $T=2.1$ are roughly the same as those for T_c but are not plotted in the figure to enhance clarity.

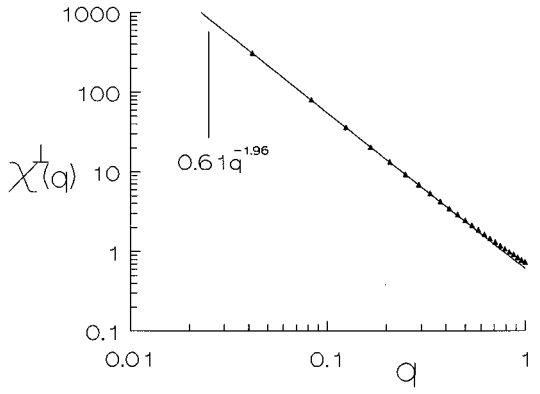

FIG. 9. log-log plot of $\chi_\xi^\perp(\mathbf{q})$ vs q showing $\chi_\xi^\perp(\mathbf{q})\propto q^{-1.96}$ as $q\to 0$ in agreement with theory.

curve at high q values could only be estimated due to the extremely broad nature of the central peak for small q. In particular, for small q the spin-wave peak was completely hidden by the central peak. The dispersion curve values we were able to obtain, however, show the decreased frequency as predicted by renormalization group theory.[4]

As a by-product of our results, though this is not a dynamic property, we obtained results for $\chi_\xi^\parallel(\mathbf{q})$ and $\chi_\xi^\perp(\mathbf{q})$. According to theoretical calculations,[17,18] $\chi_\xi(\mathbf{q})\propto q^{-(2-\eta)}$ in the limit $q\to 0$. For the case of the Heisenberg magnet, $2-\eta=\beta/\nu=1.962$.[1] Finite-size effects more pronounced than those in the transverse component caused our results not to converge for the longitudinal component. Our results for the transverse component showed finite-size effects even for the largest three lattice sizes, and so we only considered the largest lattice size ($L=48$). We found, as shown in Fig. 9, that the asymptotic regime for q was entered at $q\approx\pi/3$ where we obtained an exponent value of $2-\eta=1.960(8)$, in agreement with theory.

B. Results for dynamic scaling theory

In order to test the dynamic scaling theory we calculated $\omega_m(qL)$ using $S^\perp(\mathbf{q},\omega)$ with $qL=2\pi$ ($n=1$) for all lattice sizes. We used the transverse component only in our dynamic finite-size scaling analysis since we have found in calculating $\chi_\xi^\parallel(\mathbf{q})$ that finite-size effects are more pronounced in the longitudinal than in the transverse components. If we use all the lattice sizes to determine z from the slope of the $\log\omega_m$ vs $\log L$ plot, we get a value of approximately $z=1.4$; however, using only the three largest lattice sizes we obtained a value of $z=1.48(4)$. We then graphed $\omega_m L^z$ vs L using these two values of z and this graph is shown in Fig. 10. With the error bars on the results taken into consideration it becomes clear that in fact $z=1.48(4)$ is the correct result from our data and the asymptotic regime is reached at $L\approx 30$. This result serves as an important warning against the use of lattice sizes which are too small and also indicates the importance of the determination of accurate error bars for all simulation results. Our result of $z=1.48(4)$ is in agreement with the experimental results of Tucciarone *et al.*[9] and also validates dynamic scaling theory.

We once again used our results to test dynamic scaling through the use of Eq. (14). We graphed $S_L^k(\mathbf{q},\omega)/L^z\chi_L^k(\mathbf{q})$

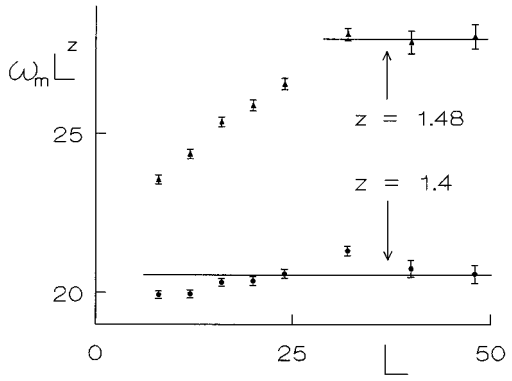

FIG. 10. Graph of $\omega_m L^z$ vs L for $z=1.4$, the dynamic critical exponent value gained from the slope of the log-log plot using all lattice sizes, and $z=1.48$, the value of the dynamic critical exponent gained from fitting only the largest three lattice sizes. The size of the error bars indicate that $z=1.48(4)$ is the correct value obtained from our results, the asymptotic regime being reached for lattice size $L=32$. Dynamic scaling theory ($z=1.5$) is thus verified. One sees the danger inherent in using lattice sizes that are too small and the importance of an accurate estimation of the error bars on all simulation results. In calculating ω_m, $n=1$ ($qL=2\pi$) was used.

vs ωL^z for the three lattice sizes found to be in the asymptotic regime with the dynamic critical exponent set to $z=1.48$. As shown in Fig. 11 the three graphs were collinear to within the bounds of their error bars, thus once again validating dynamic scaling theory. We also included the shape of the scaling function for $L=16$ in Fig. 11 to show finite-size effects in the smaller lattices.

C. Fitting data to analytical functions

We were successful in fitting $S^{\perp}(\mathbf{q},\omega)$ at temperatures below T_c to a Lorentzian form for frequency values smaller than $\omega \approx 4/J$ as shown in Fig. 12.

Tucciarone *et al.* ''successfully'' fit their experimental data to the Lorentzian form

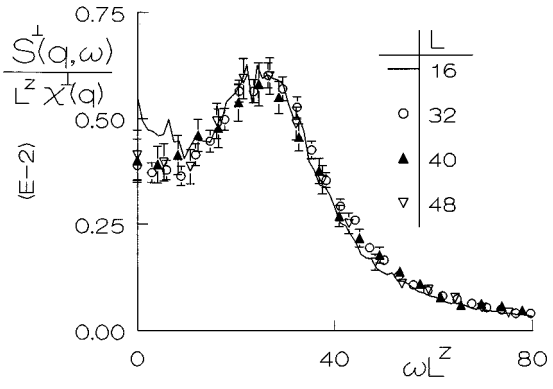

FIG. 11. Graph of scaling functions for lattice sizes $L=32,40,48$ showing the three graphs to be colinear within error bars for $z=1.48$, thus validating dynamic scaling theory. The form of the scaling function for $L=16$ is included to show the effects of finite size. $n=1$ ($qL=2\pi$) was used.

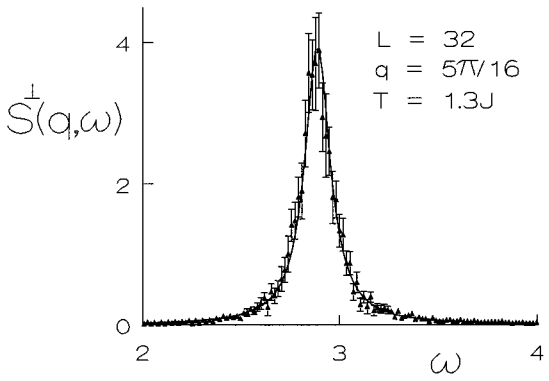

FIG. 12. Successful Lorentzian fit for $T=1.3J$, $q=5\pi/16$, and lattice size $L=32$.

$$S(\mathbf{q},\omega)=A\left(\frac{\Gamma_1}{\Gamma_1^2+\omega^2}+\frac{B\Gamma_2}{\Gamma_2^2+(\omega+\omega_s)^2}+\frac{B\Gamma_2}{\Gamma_2^2+(\omega-\omega_s)^2}\right), \tag{18}$$

where the first term is the contribution from the central peak and the last two terms are from spin-wave creation and annihilation. We found, as shown in Fig. 13, that this function did not fit the high-frequency tails of $S(\mathbf{q},\omega)$, a region not accessed by the experiment. This indicates that the Lorentzian form commonly assumed in fitting spin-wave peaks in the neutron scattering function may not be accurate in the critical regime. Attempts to fit the data at $T=2.1J$ also indi-

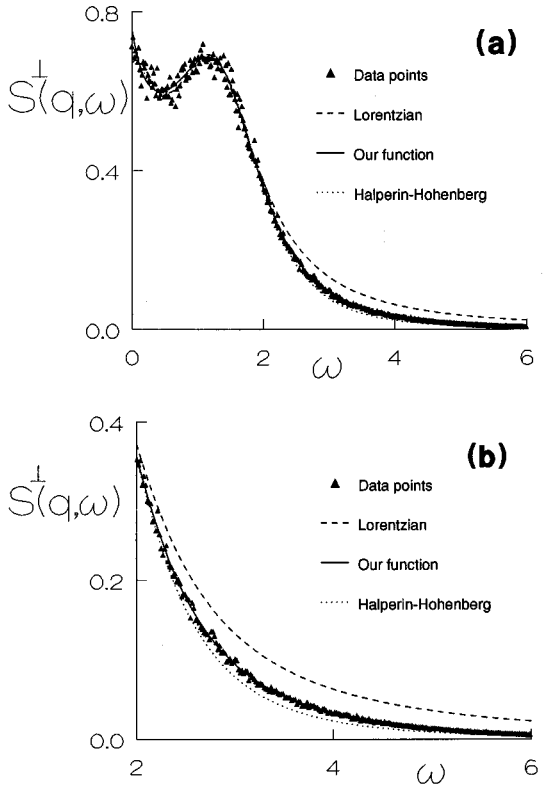

FIG. 13. Attempted fits show a lack of fit for high-frequency tails for $T=T_c$ when the spin-wave peak is fit to a Lorentzian or Halperin-Hohenberg function. This is rectified by our fitting function. In this graph $L=32$ and $q=5\pi/16$.

cate that the high-frequency tail drops off too rapidly to be fit to a Lorentzian. We then attempted to fit to a critical spin-wave peak form proposed by Halperin and Hohenberg,[12]

$$S(\mathbf{q},\omega)=A\left(\frac{\Gamma_1}{\Gamma_1^2+\omega^2}\right)+B\left(\frac{\Gamma_2}{\Gamma_2^2+(\omega^2-\omega_s^2)^2}\right), \quad (19)$$

with somewhat better but still unsuccessful results (Fig. 13). We found that the high-frequency tail drops off first as a power law and then exponentially. Equation (19) can be expressed as an inverted quartic equation. By adding an exponential term in the new quartic denomenator we were able to model this behavior. This resulted in a successful seven-parameter fit for $S^{\perp}(\mathbf{q},\omega)$ over the entire range of q values,

$$S(\mathbf{q},\omega)=(a_0+a_1\omega+a_2\omega^2+a_3\omega^3+a_4\omega^4+a_5e^{a_7\omega})^{-1}, \quad (20)$$

and this successful fit is shown in Fig. 13.

IV. CONCLUSION

In the largest spin dynamics simulation yet performed, with larger lattices, more initial configurations, and longer time development than ever before, the dynamic finite-size scaling theory developed by Chen and Landau has once again been validated. A result for the dynamic critical exponent for the bcc Heisenberg antiferromagnet of $z=1.48(4)$ was found that is in agreement with theoretical and experimental results. The asymptotic regime for the spin-wave peak was found to be entered at the large lattice size of $L\approx 30$. As a by-product of our results we found that the momentum-dependent susceptibility for transverse exitations, $\chi_{\xi}^{\perp}(\mathbf{q})$, approaches $\chi_{\xi}^{\perp}(\mathbf{q})\propto q^{-2-\eta}$ as $q\to 0$ as predicted by theory.

Below T_c we found, in agreement with experiment, the existence of a spin diffusion peak which was predominantly longitudinal and the possible existence of longitudinal multiple spin-wave peaks. The spin-wave peak narrowed and approached the linear spin-wave theory result as $T\to 0$ as expected. Above T_c we found the spin-wave peak to be at a lower frequency than the result at T_c, in agreement with theory.

We were successful in fitting the spin-wave peaks below T_c to a Lorentzian form and were also able to analytically fit the data taken at and above T_c to a function we created.

ACKNOWLEDGMENTS

This research was supported in part by NSF Grant No. DMR.9405018. The use of the Cray C90 at the Pittsburgh Supercomputer Center was supported by NSF Metacenter Grant No. MCA94P031P. We would like to acknowledge helpful discussions with Hans Gerd Evertz.

*Current address: Solid State Division, Oak Ridge National Laboratory, Oak Ridge, Tennessee 37831.

[1] K. Chen, A. M. Ferrenberg, and D. P. Landau, Phys. Rev. B **48**, 3249 (1993).
[2] P. C. Hohenberg and B. I. Halperin, Rev. Mod. Phys. **49**, 435 (1977).
[3] F. Wegner, Z. Phys. **218**, 260 (1969).
[4] R. Freedman and G. F. Mazenko, Phys. Rev. B **13**, 4967 (1976).
[5] A. Cuccoli, S. W. Lovesey, and V. Tognetti, J. Phys. Condens. Matter **6**, 7553 (1994).
[6] S. J. Pickart, H. A. Alperin, and R. Nathans, J. Phys. **25**, 565 (1964).
[7] D. T. Teaney, V. L. Moruzzi, and B. E. Argyle, J. Appl. Phys. **37**, 1122 (1966).
[8] C. G. Windsor and R. W. H. Stevenson, Proc. R. Phys. Soc. (London) **87**, 501 (1966).
[9] A. Tucciarone, H. Y. Lau, L. M. Corliss, A. Delapalme, and J. M. Hastings, Phys. Rev. B **4**, 3206 (1971).
[10] K. K. Murata, Phys. Rev. Lett. **37**, 1400 (1976).
[11] U. J. Cox, R. A. Cowley, S. Bates, and L. D. Cussen, J. Phys. Condens. Matter **1**, 3031 (1989).
[12] B. I. Halperin and P. C. Hohenberg, Phys. Rev. **177**, 952 (1969).
[13] G. F. Mazenko, M. J. Nolan, and R. Freedman, Phys. Rev. B **18**, 2281 (1978).
[14] K. Chen and D. P. Landau, Phys. Rev. B **49**, 3266 (1994).
[15] R. W. Gerling and D. P. Landau, Phys. Rev. B **41**, 7139 (1990); Proc. Phys. Soc. (London) **87**, 501 (1966).
[16] D. C. Rapaport and D. P. Landau, Phys. Rev. E **53**, 4696 (1996).
[17] S. W. Lovesey, *Theory of Neutron Scattering from Condensed Matter* (Clarendon, Oxford, 1984).
[18] D. S. Ritchie and M. E. Fisher, Phys. Rev. B **5**, 2668 (1972).